Design and Analysis of a Reflectarray Using Slot Antenna Elements for Ka-band SatCom

Qi Luo, *Member, IEEE*, Steven Gao, *Member, IEEE*, Chong Zhang, Dawei Zhou, Tobias Chaloun, Wolfgang Menzel, *Fellow, IEEE*, Volker Ziegler, *Senior Member, IEEE*, and Mohammed Sobhy

***Abstract*—This paper presents a folded reflectarray designed for Ka-band satellite communication applications. The array element is a dual-polarized slot antenna with multilayered PCB structure and is designed to operate at $29.5-30.8$ GHz band for both transmitting and receiving with single linear polarization. Vias are employed to suppress the surface wave propagation and reduce the mutual coupling between adjacent array elements, for achieving a reflectarray with a wide scan angle range. An equivalent circuit model for the array element is developed and it agrees well with the EM simulation results. Several passive demonstrators consisting of 116 elements spaced by $0.5\lambda_{30\,\mathrm{GHz}}$ were fabricated and measured. The experimental results show that the presented reflectarray is capable of steering the beam up to $\pm 60^{\circ}$ in both E- and H-planes with low cross-polarization level.**

***Index Terms*—Beam scanning, Ka-band, reflectarray, slot antenna.**

I. Introduction

THE DEMANDS for high-data-rate communication links using mobile satellite communication (SatCom) systems keep increasing. To fulfil such needs, an antenna array with beam scanning capability is required. For example, on the SatCom user terminals, the antenna is usually required to be able to scan its beam within a large angle range in order to guarantee the coverage availability. In this context, a phased array with full electronic beam scan capability, low profile, and low mass is required.

Printed microstrip array antennas have been widely used in the design of smart array antennas and beam-forming can be performed by controlling the phase and amplitude on each radiating element [1]. These antennas have the advantage of easy fabrication, low profile, and low cost. However, when there is a need to use a large number of radiating elements, the feed network becomes complicated and the power loss is high especially at millimeter-wave frequencies [2].

Recently, reflectarrays have received much research interest. They combine some of the advantages of reflector antennas and phased arrays [3]. A conventional microstrip reflectarray consists of a printed array (e.g., patch antennas), which is illuminated by a feed antenna such as a circular horn. Each radiating element is designed to provide a preadjusted phase to form a focused beam along a desired direction [4]. At its operation frequencies, a reflectarray antenna can substitute the traditional parabolic reflector with a lightweight planar structure. The phase of the reflectarray cells can be adjusted by modifying the geometry of the radiating element [5], changing the characteristics of the substrate [6], using elements of variable rotation angles [7], or using identical antenna elements with open-circuited microstrip stubs of varied lengths [8]. While conventional reflectarray has a high profile, folded reflectarray configuration has been proposed to provide a low-profile solution [9].

For mobile satellite communications, it is desirable to use an antenna that can steer the beam within large angle range. Many reported reflectarrays either only have limited beam scan range or are not suitable for integration with active microwave circuits [10]–[12]. This paper describes a folded reflectarray that is capable of steering the beam in the upper hemisphere, for the Ka-band SatCom user terminal smart array antenna within the framework of the European FP7 project FLEXWIN [13]. The objective of this work is to design a reflectarray that is capable of scanning its beam within large angle range and is suitable for integration in a multilayered manifold with phase shifters and monolithic microwave-integrated circuit (MMIC). The presented reflectarray has a multilayered PCB structure and the interface can be adapted for future integration with the transmit/receive unit [14]. Compared to the multilayered array fabricated using low-temperature co-fired ceramic (LTCC) techniques, using PCB has the advantage of lower fabrication cost and accessing many low dielectric constant materials. A folded reflectarray is chosen in this study due to its advantage of low profile compared to the conventional reflectarray. Fig. 1(a) and (b) shows the configuration of a conventional reflectarray and a folded reflectarray, respectively. A folded reflectarray usually consists of a feed antenna, radiating elements with preadjusted phase for focusing the beam, and a polarizer grid. As can be seen from Fig. 1(b), for the folded reflectarray, the feed horn is linearly polarized and the radiated wave from the feed horn is reflected back by the polarizer. Then, the wave is incident on the reflectarray and reradiates with the

Manuscript received March 13, 2014; revised January 21, 2015; accepted February 03, 2015. Date of publication February 06, 2015; date of current version April 03, 2015. This work was supported by EC FP7 under the "FLEXWIN" project.

Q. Luo, S. Gao, and M. Sobhy are with the School of Engineering and Digital Arts, University of Kent, Canterbury CT2 7NT, U.K. (e-mail: qiluo@ieee.org; s.gao@kent.ac.uk).

C. Zhang is with the Northwestern Polytechnical University, Xi'an 710072, China.

D. Zhou was with the University of Surrey, Surrey, U.K. He is now with Huawei Device Ltd., Beijing 100083, China (e-mail: daweizhou@hotmail.com).

T. Chaloun and W. Menzel are with the Institute of Microwave Techniques, University of Ulm, Ulm D89069, Germany.

V. Ziegler is with Airbus Group Innovations, Munich D81663, Germany.

Color versions of one or more of the figures in this paper are available online at http://ieeexplore.ieee.org.

Digital Object Identifier 10.1109/TAP.2015.2401393

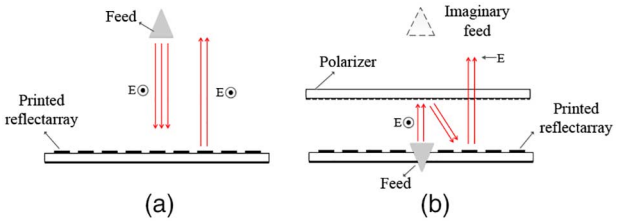

Fig. 1. Configuration of (a) conventional reflectarray array and (b) folded reflectarray.

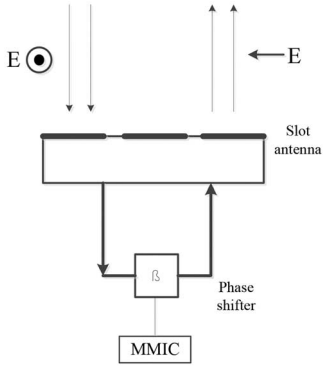

Fig. 2. Demonstration of using the proposed dual-polarized element to rotate the E-field and incorporated with the phase shifters and MMIC.

electric field rotated by 90°. This is equivalent to having an imaginary feed above the center of the reflectarray.

To realize the 90° rotation of the electric field, conventionally, rectangular patches are used for the design of the reflectarray unit cell and the patch axes are tilted by 45° with respect to the incident electric field [15], [16]. However, this method cannot be applied to design an active beam-steering folded reflectarray because the phase of each radiating element is fixed by its physical dimensions. In this work, a dual-polarized slot antenna element is employed as the reflectarray unit cell. The rotation of the electric field by 90° can be obtained when two ports of the antenna are connected. This approach provides a feasible solution to integrate the folded reflectarray to the MMIC with phase shifters, as demonstrated in Fig. 2. To our best knowledge, there has been few works reported in this field of using dual-polarized elements to design a folded reflectarray that is suitable for a highly integrated solution. One of the challenges is that besides realizing dual linear polarization, there must be high isolation between the two ports of the array unit cell. Moreover, to avoid grating lobes at large scan angles, the spacing between adjacent radiating elements is chosen to be $0.5\lambda_{30\,\mathrm{GHz}}$, where $\lambda_{30\,\mathrm{GHz}}$ is the free space wavelength at 30 GHz. Another novelty of this work is the reduced number of vias introduced to decrease the mutual coupling between the neighboring elements. By carefully choosing the positions of the vias, the isolation between adjacent antenna elements and the two ports of the array unit cell is kept very low. This improves the scan performance of the array.

A prototype of the dual-polarized slot antenna was fabricated for the purpose of characterizing the reflectarray unit cells. Several passive reflectarray demonstrators with fixed beam angles were also fabricated to verify the radiation performance

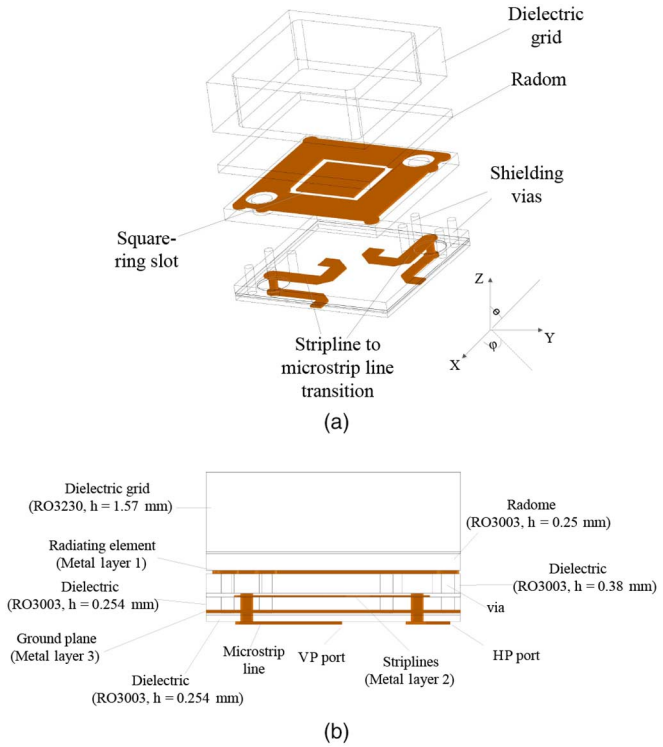

Fig. 3. (a) Exploded and (b) side view of the reflectarray element. Some vias are not shown for figure clarity.

of the presented folded reflectarray and ensure that when a proper beam forming network is incorporated, the reflectarray is able to steer the beam within the angle range of $\pm 60°$.

This paper is organized as follows. Section II presents the design and characterization of the slot antenna element. In Section III, the equivalent circuit model of the multilayer ring-slot antenna is described. The array performance analysis and the descriptions of reflectarray design are presented in Sections IV and V, respectively. The experimental results are given in Section VI. Section VII concludes the paper.

II. Design and Characterization of the Slot Antenna Element

A. Configuration of the Slot Antenna Element

The structure of the antenna element is presented in Fig. 3. Since the element is designed for a folded reflectarray, the antenna unit cell is required to be able to rotate the polarization of the incident wave by 90°, as indicated in Fig. 1(b). A dual-polarized square-ring slot antenna is chosen for this design due to its compact size and symmetrical geometry. The size of the antenna unit cell is $0.5\lambda_{30\,\mathrm{GHz}} \times 0.5\lambda_{30\,\mathrm{GHz}}$. Compared to the dual-polarized reflectarray unit cell presented in [17], this antenna element has a simpler structure with symmetrical configuration and, as will be presented later, it exhibits good impedance matching and stable central resonance frequency at different scan angles.

The ring-slot was printed on a 0.38-mm thick Rogers RO3003 substrate with a relative dielectric constant (ε_r) of 3. The detailed dimensions of this slot antenna are given in

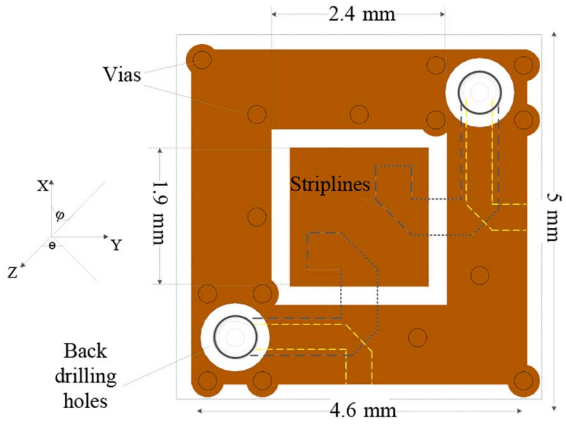

Fig. 4. Top view of the square-ring slot radiating element with dimensions.

Fig. 4. As can be seen from Fig. 3, the antenna element has a multilayered structure. Rogers 3001 ($\varepsilon_r = 2.28$) bonding films were used to bond the layers together. To ensure that the antenna element is suitable for future integration with the MMIC, which is placed at layers below the radiating element, striplines were chosen to load the slot antenna. Then, a vertical RF transition from stripline to coaxial can be employed to connect the stripline of the slot antenna to the MMIC. For the purpose of characterizing the radiating element, in the first stage, a vertical RF transition from stripline to microstrip was used.

Horizontal polarization (HP) or vertical polarization (VP) of the antenna can be selected by exciting the corresponding ports. The HP port is defined as the port on the Y-axis, whereas the port on the X-axis is referred as the VP port. With this configuration, the microstrip lines of the antenna, which were used for the antenna element characterization, can be printed on the layer below the ground plane of the stripline, thus avoiding the unwanted radiation from the microstrips.

Shorting vias were placed close to the ring slot to reduce the mutual coupling between the array elements, improve the isolation between the two ports, and eliminate the undesired parallel-plate mode between metal layers 1 and 3. As will be presented in the next section, the isolation between the two ports as well as the isolation between adjacent elements were improved significantly after the introduction of these vias.

A 0.25-mm thick Rogers RO3003 substrate was used as the radome of the slot antenna, for the purpose of removing some susceptance variation when the array scans and thus improving its impedance matching at different scan angles [18]. An additional dielectric grid made of 1.57-mm thick Rogers RO3203 ($\varepsilon_r = 3.02$) was added on top of the radome. Having a thick dielectric can excite the propagation of surface waves, which is undesirable for the design of an antenna array. In our study, it is found that with a dielectric grid, a compromise between low surface wave propagation and impedance matching can be achieved. As will be presented in Section V, with this dielectric grid, there is good impedance matching of the array at different scan angles. The size and thickness of the dielectric grid was optimized by performing numerical simulations, considering the availability of the commercially available low-permittivity substrates.

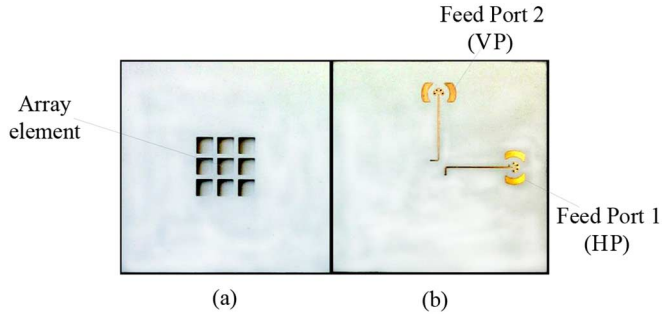

Fig. 5. (a) Top and (b) back views of the fabricated 3 × 3 finite array.

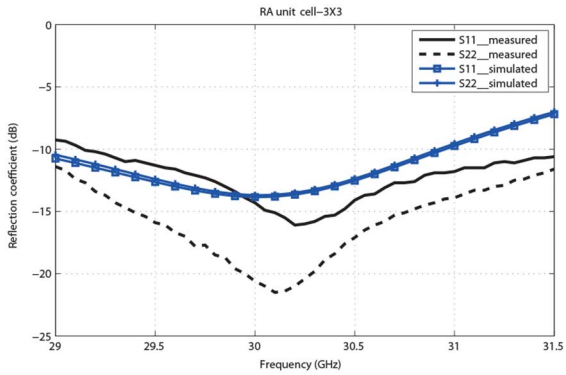

Fig. 6. Simulated and measured reflection coefficients of the array element.

B. *Characterization of the Slot Antenna Element*

To measure the reflection coefficient and isolation of the array element, a 3 × 3 finite array was fabricated and characterized as a classic direct radiating array fed by microstrip lines. Due to the small size of the array unit cell, it is only possible to include two MMPX PCB connectors to feed the two ports of the central radiating element through the stripline to microstrip transitions. The rest of array elements were loaded with open striplines. Since there is very high isolation between the adjacent radiating elements (see Fig. 8), each unit cell of the array can be treated as an independent cell. Therefore, the results measured from a small size finite array are valid.

Fig. 5 shows the photos of the fabricated prototype. The simulated and measured reflection coefficients of the antenna element were compared and presented in Fig. 6. Both the simulated and measured reflection coefficients indicate that the slot antenna has 10-dB return loss bandwidth from 29 to 31 GHz. Fig. 7 shows a comparison between the simulated and the measured isolation between the two ports of the array element. Within the frequency band of interest, the isolation is always better than 20 dB. The simulations were performed by simulating a 3 × 3 finite array with all the ports activated. All the simulations shown in this paper were performed using commercial 3-D EM simulation software package Ansys HFSS (high-frequency structure simulator) [19].

The measured results were obtained using a TRL (Thru, Reflect, Line) calibration kit [20]. As can be seen from Figs. 6

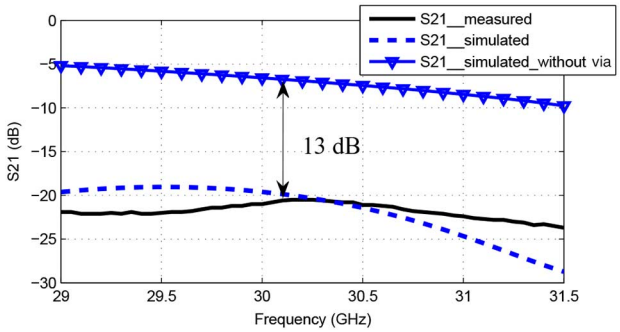

Fig. 7. Simulated and measured isolation between the two ports of the array element.

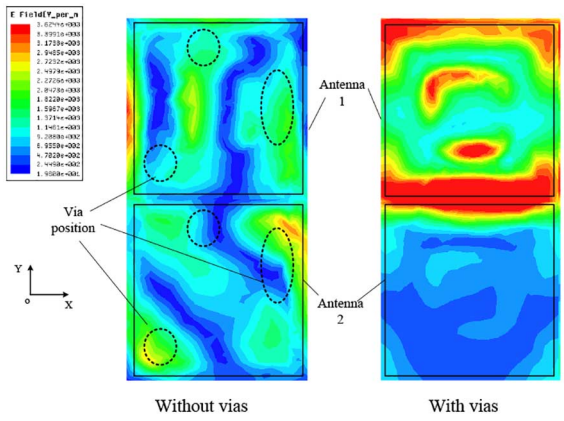

Fig. 8. Simulated E-field in the XoY plane of a two-element array with and without the vias when only one antenna is radiating.

and 7, there is a good agreement between simulated and measured reflection coefficients in terms of central resonance frequency and 10-dB return loss bandwidth. There is less than 3-dB difference between the simulated and the measured isolation. These differences are mainly due to the fabrication accuracy including the alignment of the layers and the position of the plated through holes.

Vias were introduced to suppress the propagation of the surface waves and thus improve the isolation between the two ports of the radiating element as well as the isolation between different radiating elements. The initial positions of the vias were chosen to be at the regions where the strongest E-field exists without interfering with the radiation from the slot antenna. To explain this better, Fig. 8 shows the simulated E-field in the XoY plane of a linear array with two antenna elements when only the antenna on top is radiating. From Fig. 8, it can be observed that without any vias, there is a strong mutual coupling between these two antennas. After introducing the vias at the positions indicated in Fig. 8, the propagation of the surface current was greatly suppressed, thus high isolation between array elements can be obtained. It is important to ensure that after introducing the vias, there is little influence on the impedance matching of the antenna, so it is not recommended to introduce many vias, which is also constrained by the small size of the unit cell and fabrication accuracy. Numerical simulations were performed to optimize the positions and number of the vias in order to get the highest isolation

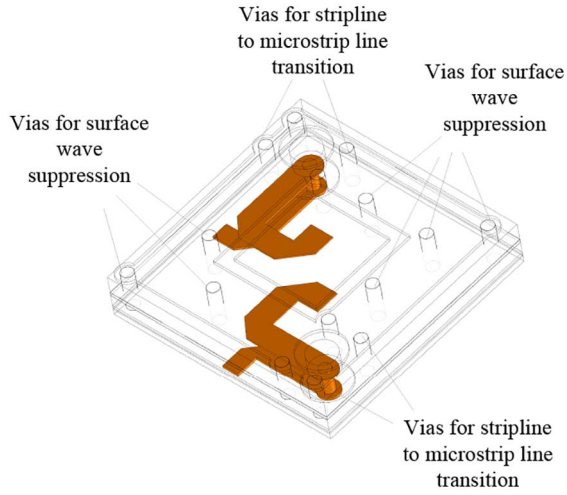

Fig. 9. Layout of the square-ring slot radiating element.

between adjacent radiating elements with as few vias as possible. The positions of the vias are shown in Fig. 9. Because of the symmetry of the antenna unit cell, the obtained results from the linear two-element array can be applied to the planar array.

Fig. 7 also compares the simulated isolation between the HP and VP ports with and without introducing the shorting vias. It can be seen that with the existence of these vias, there is a minimum 13-dB improvement in the isolation between the two ports.

III. Equivalent Circuit Analysis of the Multilayer Slot Antenna

The equivalent circuit of the slot antenna has been developed, in order to understand better the operation principle of the radiating element. Due to the complexity of the multilayered structure and the inhomogeneous nature of the substrates caused by the vias (vias are realized by plated through holes), which are filled with bonding dielectric material, after the circuit models are derived and the initial values of the lumped elements are calculated, curve fitting technique is adopted to perform the parameter tuning.

A. Stripline to Microstrip Transition

Fig. 10(a) shows the side view of the stripline to microstrip line transition structure and its equivalent circuit model. The central via and its shielding can be regarded as a coaxial cable and C_1, L_1 are evaluated using the equations given in [21]

$$C = \frac{2\pi h \varepsilon_0 \varepsilon_r}{\ln\left(\frac{D}{d}\right)} \tag{1}$$

$$L = \frac{h\mu_0\mu_r}{2\pi} \times \ln\left(\frac{D}{d}\right) \tag{2}$$

where h is the height of the central via, d is the outside diameter of central via, D is the inside diameter of the shielding, ε_0 is the permittivity of the free space, ε_r is the

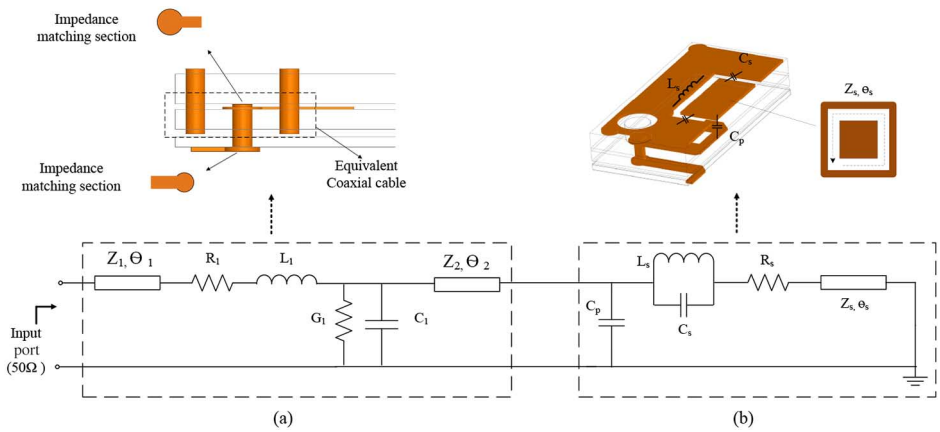

Fig. 10. Equivalent circuit model of the (a) stripline to microstrip transition and (b) ring-slot antenna.

relative dielectric constant of the material, μ_0 is the permeability of free space, and μ_r is the relative permeability of the material.

The series resistance R_1 is the loss resistance of the inner conductor and the shunt conductance G_1 represents the loss in the dielectric. In this study, because the inner conductor has a length of only 0.25 mm and the dielectric has a loss tangent of only 0.0013, both elements can be neglected due to their small values. The impedance matching section is a circular stub that connects the stripline to the microstrip through the vertical via. The radius of the circular stub can be tuned to optimize the impedance matching of the stripline to microstrip transition. The impedance matching section at the transitions were modeled as two transmission lines Z_1, θ_1 and Z_2, θ_2, where Z and θ represent the characteristic impedance and electrical length of the transmission line, respectively. The initial values of the circular stub can be calculated using classic transmission line theory.

In this design, the diameter of the central via is 0.25 mm, the diameter of the shielding is 1.44 mm, and the height of the central via is 0.254 mm. This corresponds that C_1 equals 0.04 pF and L_1 equals 87 pH. By performing curve fitting with the EM simulation results, Z_1, θ_1, Z_2, θ_2 were optimized to be 38 Ω, 104°, 62 Ω, 150°, respectively.

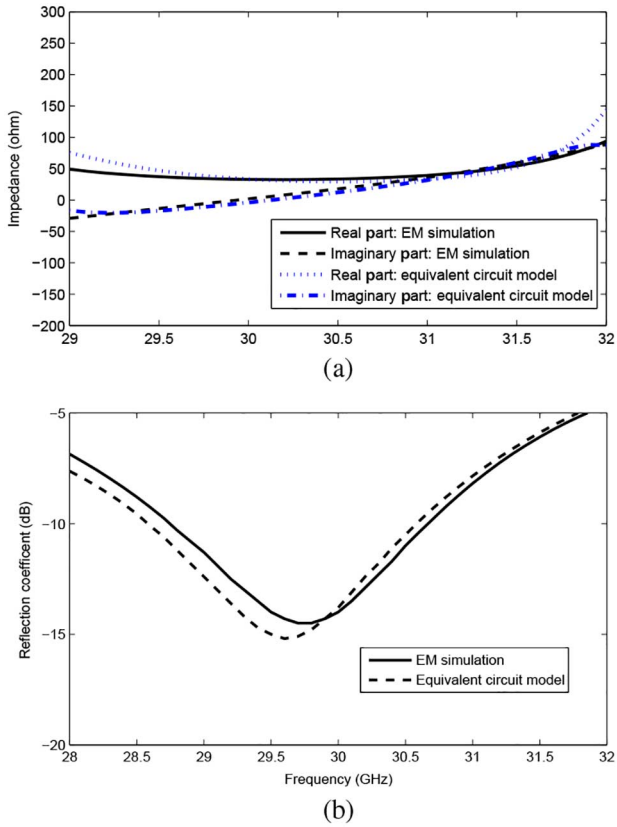

Fig. 11. Comparison of (a) input impedance and (b) reflection coefficient obtained from the full-wave simulation and the equivalent circuit model.

B. Slot Antenna

Fig. 10(b) presents the sectional view of the square-ring slot antenna fed by single stripline and its corresponding equivalent circuit model. As indicated in Fig. 10(b), the capacitor C_p is the shunt capacitance of the feed line when it crosses the ring slot. L_s and C_s are the inductance and capacitance of the slot. The resistor R_s represents the radiation resistance and ohmic loss of the slot antenna, and Z_s and θ_s are the characteristic impedance and electrical length of the slot line. The initial values of Z_s and θ_s can be calculated using slot line theory, where the impedance of a slot line is given by the formulas provided in [22]. At the resonance frequency, two conditions must be simultaneously satisfied: the *LC* circuit is in the condition of resonance while the circumference of the ring slot has a electrical length approximately one wavelength. Therefore, by cascading the *LC* circuit with a transmission line, the radiation characteristics of the slot antenna can be well represented.

After placing the circuit model of the slot antenna as the termination of the circuit model of the microstrip to stripline transition structure, other values of the circuit components were extracted by performing curve fitting with the EM simulation results: C_p is 0.01 pF, C_s is 0.62 pF, L_s is 25 nH, R_s is 24.5 Ω, Z_s is 41.6 Ω, and θ_s is 380°. Fig. 11 shows the comparison between the input impedance of the slot antenna from the full wave simulation and the calculated results using the equivalent

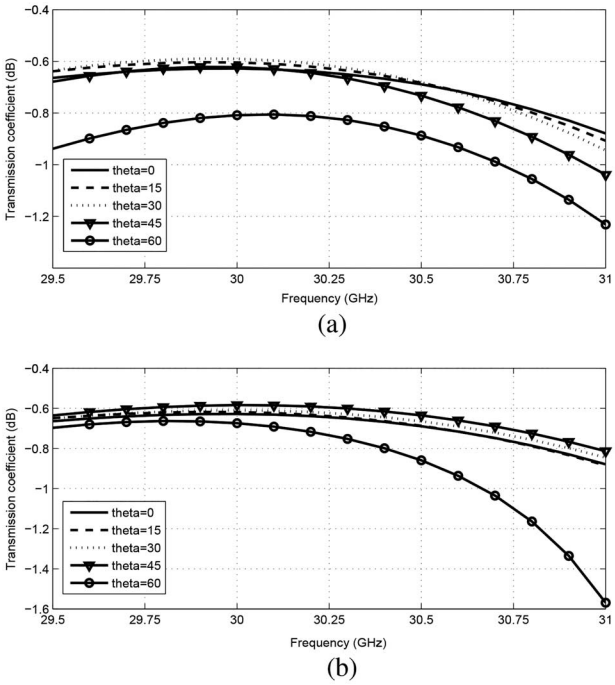

Fig. 12. Transmission coefficient of the array in (a) $\phi = 0^\circ$ plane and (b) $\phi = 90^\circ$ plane when it scans.

circuit model with a 50-Ω port. As seen, good agreement is obtained.

IV. Array Performance Analysis

A. Array Scanning Performance Analysis Using Floquet Mode

The scanning performance of the array unit cell was studied using Ansys HFSS with the Floquet port to simulate an array of infinite size. Fig. 12 shows the simulated scanning performance of the infinite large reflectarray using the dual-polarized slot antenna as array element. During the simulation, the antenna element shown in Fig. 3 was calculated with periodic boundary condition and the transmission coefficient was extracted from the ports of the unit cell between the Floquet port, which can be used to evaluate the loss performance of the infinite size array with different scan angles. The approach is accurate when the size of the finite array is large. From these simulation results, it is observed that the transmission loss of the array is less than 1.2 dB when it scans up to 60° within the frequency band of interest in both E- and H-planes. This proves that using this unit cell, the array is able to steer the beam to large angles.

The mutual coupling between array elements should be minimized to reduce the effect of the mutual impedance variations when the array scans [23]. To ensure that there is high isolation between the radiating elements, it is important to simulate the antenna array before fabrication. However, simulating an array of large size is not feasible because it requires large computational resources and leads to long simulation time. Instead, a finite size array consisting of 3×3 array elements was simulated. Although the size of the array is small, the simulated results for the central element is still valid, because the adjacent elements contribute to most of the mutual coupling. The

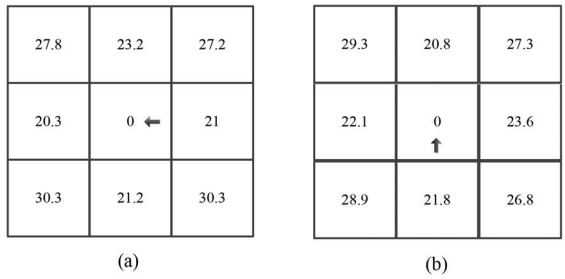

Fig. 13. Isolation (unit is in dB) between adjacent elements when (a) HP and (b) VP ports are excited.

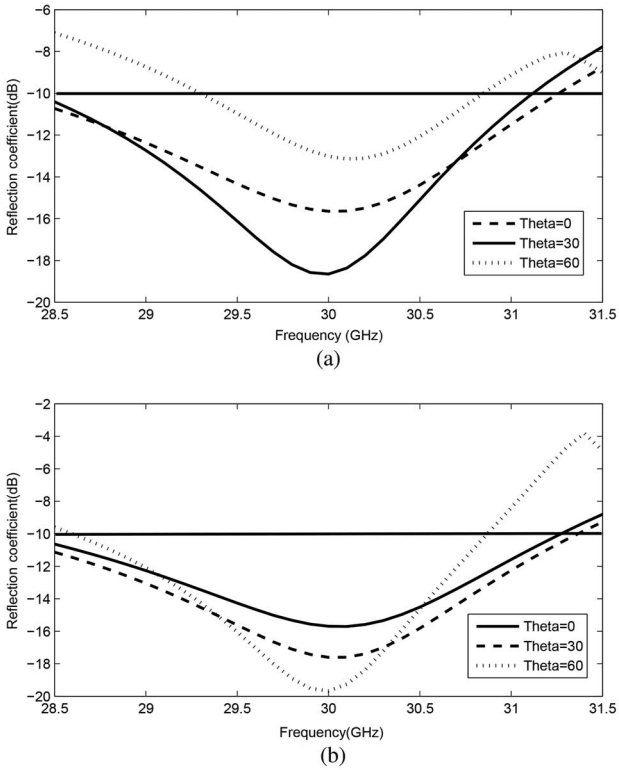

Fig. 14. Simulated reflection coefficient of the array when it scans in the (a) $\phi = 0^\circ$ and (b) $\phi = 90^\circ$ planes.

isolation between the central element and the adjacent eight elements was extracted from the simulated scattering matrix and are given in Fig. 13. During the simulations, only the antenna in the central position was excited, and the rest of the radiating elements were loaded with $50\,\Omega$ ports. As can be seen from the simulation results, the isolation is always better than 20 dB when either the HP or VP port is excited.

The scanned reflection coefficient of the array element in a infinite array is presented in Fig. 14. It is found that good impedance matching and stable central resonance frequency is obtained when the array scans at both $\phi = 0^\circ$ and $\phi = 90^\circ$ planes. This is due to that there are low mutual couplings between array elements and the use of the dielectric grid on top of the radome layer. Considering the results shown in Fig. 12, at large scan angles, the transmission coefficient decreases, so some losses in the structure (e.g., dielectric loss) are anticipated.

B. Scan Blindness

The scan blindness of an array is caused by the cancelation of the dominant mode by the higher modes of the radiating element [24]. Scan blindness is also related to a true surface wave supported by the antenna structure [18]. The blind angle of the array can be determined using the Floquet modal functions. Scan blindness takes place when the wavenumber of the surface wave matches with the wavenumber of the Floquet mode. This means that there is a strong coupling between the surface wave and the Floquet mode. Since a rectangular grid is employed in this study and it is known that (0,0) is the dominant Floquet mode, the following equations are derived from [25]

$$k_{\rho s}\cos\alpha + \frac{2m\pi}{a} = k_0 \sin\theta_{\text{blind}}\cos\phi \tag{3}$$

$$k_{\rho s}\cos\alpha + \frac{2n\pi}{b} = k_0 \sin\theta_{\text{blind}}\sin\phi \tag{4}$$

where θ_{blind} is the scan blindness angle and m, n is the mode number. Solving the two equations, a new expression for the scan blindness angle in the E-plane is derived

$$\begin{aligned}\theta_b = \arcsin\Bigg(&\frac{1}{k_0 ba}(2b\cos(\phi)m\pi + 2a\sin(\phi)n\pi \\ &- (4b^2\cos(\phi)^2m^2\pi^2 + 8b\cos(\phi)m\pi^2 a\sin(\phi)n \\ &+ 4a^2\sin(\phi)^2n^2\pi^2 - 4b^2m^2\pi^2 + k_{ps}^2a^2b^2 \\ &- 4a^2n^2\pi^2)^{\frac{1}{2}})\Bigg).\end{aligned} \tag{5}$$

$k_{\rho s}$ is estimated by the following expression when the antenna elements are printed on a relatively thin substrate [26]

$$k_{\rho s} \approx k_0\left[1 + 0.5\left(k_0 h\left(1 - \frac{1}{\varepsilon_r}\right)\right)^2\right]. \tag{6}$$

The blind scan angle is determined by solving (5) provided that the chosen surface wave modes (m, n) can result in a valid solution. With the configuration of our array, the scan blind angle is 80.1° at 30 GHz in the E-plane, caused by the $(1, 0)$ surface modes. Because the mutual coupling between array element is lower in H-plane, the scan blind angle in H-plane is expected to be larger than 80.1°.

V. Design of the Reflectarray

The dual linearly polarized square-ring antenna presented in the previous section was used for the design of the folded reflectarray. A total of 116 elements were employed to form a circular aperture and a circular horn is placed in the central position. There is a 16-mm distance between the polarizer and the top surface of the reflectarray. The polarizer is constituted by paralleled microstrips of 0.26 mm wide spaced by 0.15 mm. Fig. 15 shows the 3-D view of the folded reflectarray.

To realize the beam forming of the passive reflectarray demonstrators, the phase delay on each array element was achieved by connecting the two ports (VP and HP) of the array element by microstrip delay lines of varied lengths. Three types of phase delay lines were developed and are shown in Fig. 16. By varying the corresponding parameters as indicated in Fig. 16, the length of the delay lines can be adjusted. As shown in Fig. 17, each type of phase delay line can provide phase delays in a different range and a total linear phase delay of up to 430° can be achieved. In this design, because the folded reflectarray has a central feed with a reasonable focal distance, similar to the conventional central-fed reflectarray, only considering the normal incident waves can provide a good approximation [4]. The phase delays are achieved by varying the length of the microstrip delay lines, which has no impact on the resonance frequency of the antenna. Fig. 17 also shows the loss of the reflected wave at 30 GHz when these three types of phase delay lines were used. The loss of the unit cell is between 1 and 1.5 dB. One main factor that contributes to this loss is the two stripline to microstrip transitions (as shown in Fig. 18) in a multilayered configuration, which introduces at least 0.8 dB losses. Another factor contributing to the loss is the impedance mismatching from the bends of the microstrips.

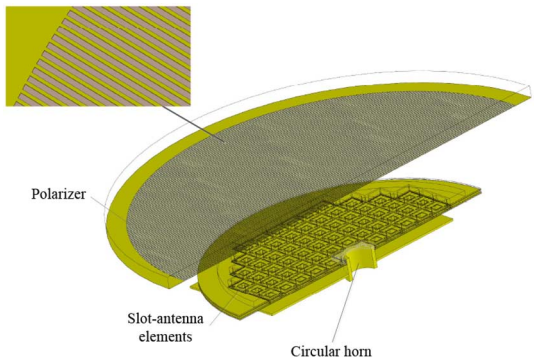

Fig. 15. 3-D sectional view of the folded reflectarray.

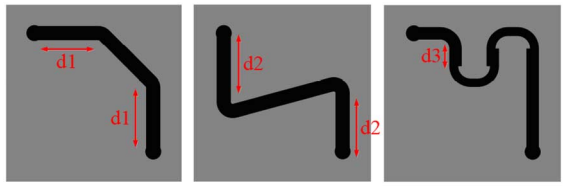

Fig. 16. Three types of microstrip phase delay lines employed in the passive reflectarray demonstrators.

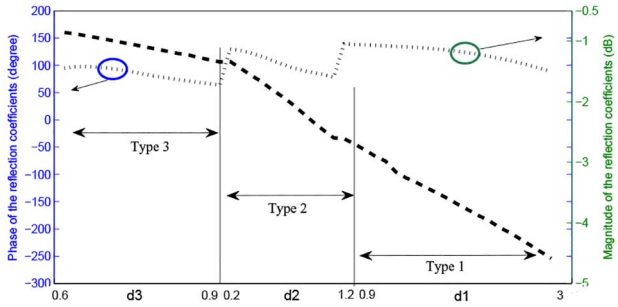

Fig. 17. Simulated phase and amplitude response of the unit cell with three types of microstrip delay lines.

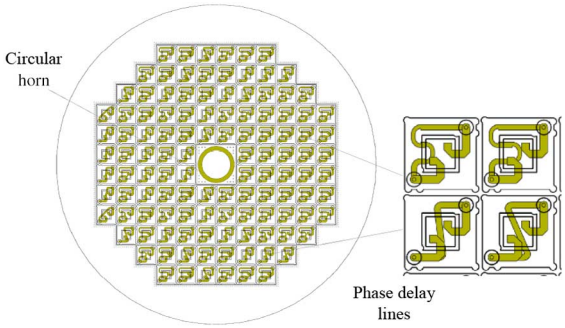

Fig. 18. Back view of the passive folded reflectarray.

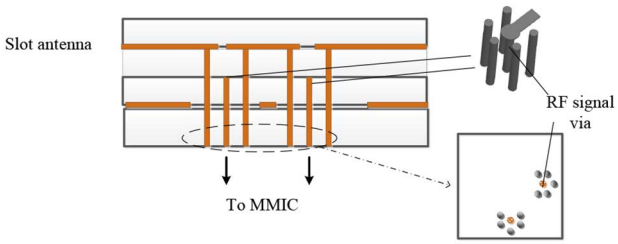

Fig. 19. Manifold that the presented reflectarray can be integrated.

Fig. 18 shows the back view of one passive reflectarray with microstrip delay lines. The required phase for each radiating element is calculated using the formula given in [4]

$$\phi_R = k_0(d_i - (x_i \cos\varphi_b + y_i \sin\varphi_b)\sin\theta_b) \qquad (7)$$

where ϕ_R is the phase of the reflection coefficient of the antenna element i, k_0 is the phase constant in vacuum, (x_i, y_i) are the coordinates of the array element i, d_i is the distance from the phase centre of the feed to the antenna unit cell, and (θ_b, φ_b) is the expected scan angles of the beam in the spherical coordinate system.

Passive models were developed to evaluate the beam-scanning capability of the presented reflectarray. The interface of the reflectarray can be adapted for future system integration. For satellite-tracking application, this reflectarray can be incorporated with phase shifters and MMIC by stripline to coaxial transitions, as demonstrated in Fig. 19. The phase of each radiating element is then adjusted by the corresponding phase shifter controlled by the MMIC and beam-steering can be realized continuously.

VI. Experimental Results of the Folded Reflectarray

Fig. 20 shows the fabricated prototype of the folded reflectarray. The thickness of the multilayered PCB is 2.85 mm. A thin plastic ring was used as the spacer for the reflectarray and the polarizer. Another plastic ring was employed as an inner spacer to separate the reflectarray and the bottom ground plane, to avoid back radiation from the microstrip phase delay lines.

Five passive reflectarray demonstrators were fabricated to verify the beam scan capability. Fig. 21 shows the measured far-field radiation patterns for the demonstrators with three different scan angles (0°, 45°, and 60°) in $\phi = 0°$ plane. In this case, only the measured E-plane radiation patterns are shown for the best interest. It is observed that the main beam of the reflectarray is able to be steered to 60° with low sidelobe level.

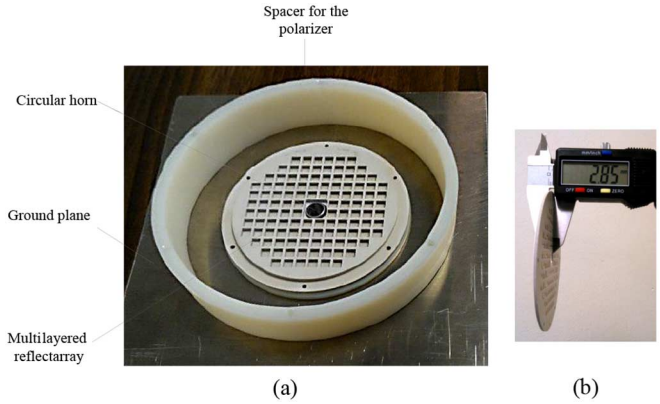

Fig. 20. (a) Fabricated prototype of the folded reflectarray. The polarizer is removed to show in the structure inside. (b) Side view of the fabricated radiating array.

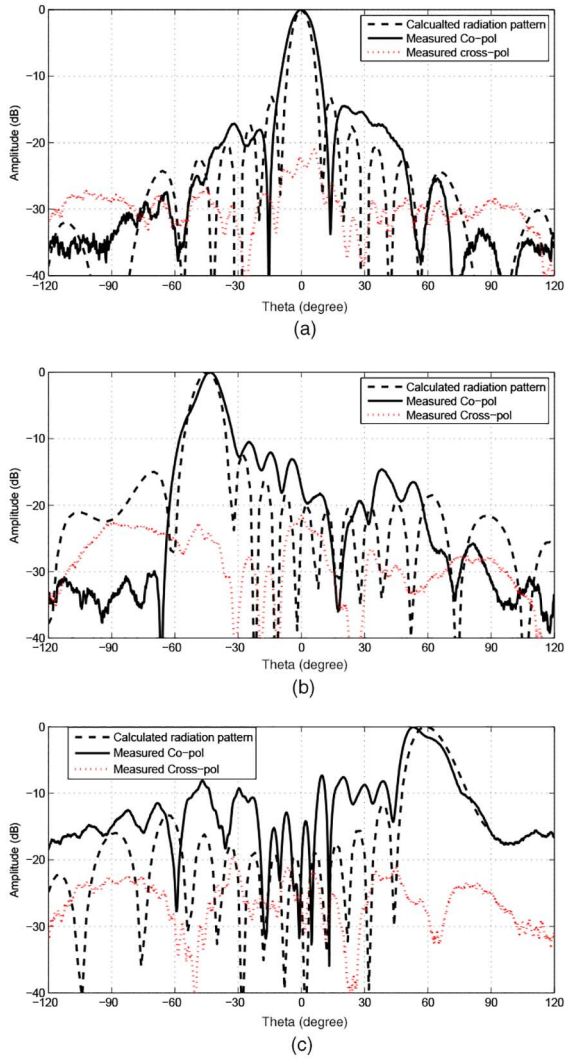

Fig. 21. Measured and calculated normalized E-plane radiation patterns of the demonstrators with beam scanned to (a) $\theta = 0°$; (b) $\theta = 45°$; and (c) $\theta = 60°$ in the $\phi = 0°$ plane.

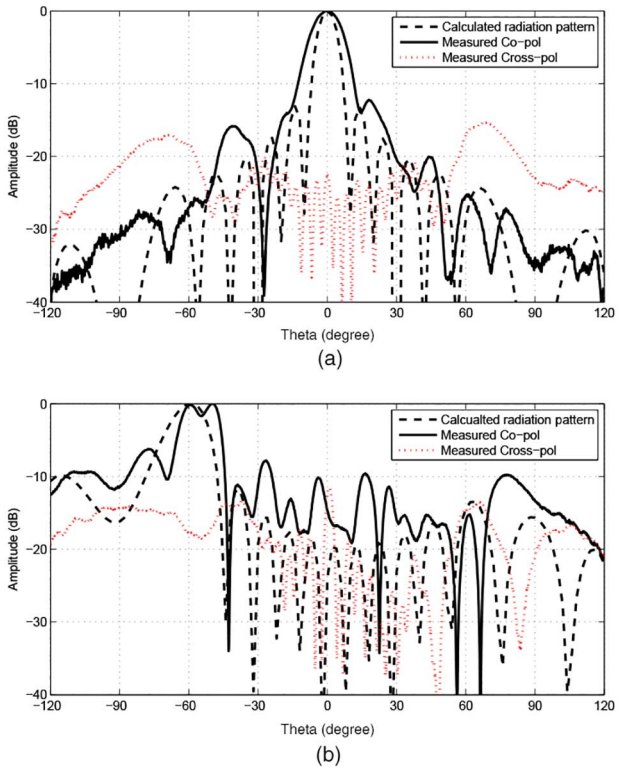

Fig. 22. Measured and calculated normalized H-plane radiation patterns of the demonstrators with beam scanned to (a) $\theta = 0°$ and (b) $\theta = 60°$ in the $\phi = 90°$ plane.

There is about 3-dB gain drop when the reflectarray scans to 60° and this is due to the reduction of the effective radiating area. The measured results also show that the cross-polarization is at least 20 dB lower than the copolarization in the direction where the focused beam is.

Fig. 22 shows the measured far-field radiation patterns for the reflectarrays with scan angles of 0° and 60° in $\phi = 90°$ plane. In this case, only the measured H-plane radiation patterns are presented. The measured results show that the cross-polarization is at least 20 dB lower than the copolarization when the reflectarray radiates at broadside. With the focused beam pointing at 60°, the cross-polarization is 15 dB lower than the copolarization. Higher sidelobes are also observed, which is due to the fact that the mutual coupling of the array element is higher in the $\phi = 90°$ plane. These results are consistent with the simulation results from the Floquet modes study presented in Fig. 12. The calculated radiation patterns are also shown in Figs. 21 and 22. During the calculation, it is assumed that all the radiating elements were excited with equal amplitude currents. In general, there are good agreements between the theoretical results and the measured ones, except that the measured results show relatively higher sidelobes levels, which is mainly due to the small misalignment of the polarizer and measurement accuracy.

The measured maximum gain of the passive demonstrator is 21.7 dBi when it has a focused beam at broadside. The aperture efficiency of this reflectarray is calculated to be 42% with an aperture radius of 30 mm. The aperture efficiency can be improved by optimizing the illumination efficiency and reducing spillover loss. Table I summarizes these measured results. Fig. 23 shows the measured gain variation of all the fabricated demonstrators. Within the frequency band of interest, the gain variation is less than 1.8 dB.

TABLE I
MEASURED RADIATION PERFORMANCE OF THE DEMONSTRATORS

	Beam angle	Measured gain (dBi)	X-pol level (dB)
Demo 1	$\theta = 0°, \phi = 0°$	21.7	–21
Demo 2	$\theta = 45°, \phi = 0°$	21.2	–23.6
Demo 3	$\theta = 60°, \phi = 0°$	18.4	–21.4
Demo 4	$\theta = 0°, \phi = 90°$	21.5	–22.5
Demo 5	$\theta = 60°, \phi = 90°$	16.2	–16

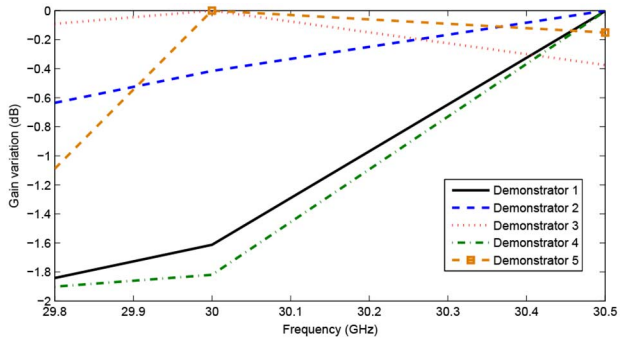

Fig. 23. Measured gain variation against the frequency of the five reflectarray demonstrators.

VII. CONCLUSION

A folded linearly polarized reflectarray for Ka-band SatCom user terminal smart antenna is presented in this paper. The folded reflectarray has a low profile and can be integrated with phase shifters and MMIC in a multilayered manifold. Square-ring slot antenna is chosen as the array element and it exhibits high isolation between adjacent elements with a few vias. The design and analysis of this array element is presented with the equivalent circuit model. Both the analysis and experimental results of the passive demonstrators suggest that the presented folded reflectarray has large scan angles and exhibits good impedance matching, low cross-polarization level, stable gain, and moderate efficiency over the required frequency band when the reflectarray has the focused beam at different scan angles.

ACKNOWLEDGMENT

The authors would like to thank Optiprint for the prototype fabrication and MIPOT for prototype assembling. They would also like to thank Prof. X. Chen and Dr. M. Candotti (Queen Mary, London) for their help during the antenna characterization.

REFERENCES

[1] S. R. Rengarajan, M. S. Zawadzki, and R. E. Hodges. "Design, analysis, and development of a large ka-band slot array for digital beam-forming application," *IEEE Trans. Antennas Propag.*, vol. 57, no. 10, pp. 3103–3109, Oct. 2009.

[2] D. M. Pozar, S. D. Targonski, and H. D. Syrigos, "Design of millimeter wave microstrip reflectarrays," *IEEE Trans. Antennas Propag.*, vol. 45, no. 2, pp. 287–296, Feb. 1997.

[3] S. V. Hum and J. Perruisseau-Carrier, "Reconfigurable reflectarrays and array lenses for dynamic antenna beam control: A review," *IEEE Trans. Antennas Propag.*, vol. 62, no. 1, pp. 183–198, Jan. 2014.
[4] J. Huang and J. A. Encinar, *Reflectarray Antennas*. Hoboken, NJ, USA: Wiley, 2007.
[5] J. Ethier, M. R. Chaharmir, J. Shaker, and D. Lee, "Development of novel low-cost reflectarrays [antenna applications corner]," *IEEE Antennas Propag. Mag.*, vol. 54, no. 3, pp. 277–287, Jun. 2012.
[6] M. Y. Ismail *et al.*, "Phase agile reflectarray cells based on liquid crystals," *IET Microw. Antennas Propag.*, vol. 1, no. 4, pp. 809–814, Aug. 2007.
[7] J. Huang and R. J. Pogorzelski, "A ka-band microstrip reflectarray with elements having variable rotation angles," *IEEE Trans. Antennas Propag.*, vol. 46, no. 5, pp. 650–656, May 1998.
[8] E. Carrasco, M. Barba, and J. A. Encinar, "Design and validation of gathered elements for steerable-beam reflectarrays based on patches aperture-coupled to delay lines," *IEEE Trans. Antennas Propag.*, vol. 59, no. 5, pp. 1756–1761, May 2011.
[9] W. Menzel, D. Pilz, and M. Al-Tikriti, "Millimeter-wave folded reflector antennas with high gain, low loss, and low profile," *IEEE Antennas Propag. Mag.*, vol. 44, no. 3, pp. 24–29, Jun. 2002.
[10] O. Bayraktar, O. A. Civi, and T. Akin, "Beam switching reflectarray monolithically integrated with RF MEMS switches," *IEEE Trans. Antennas Propag.*, vol. 60, no. 2, pp. 854–862, Feb. 2012.
[11] F. Venneri, S. Costanzo, and G. Di Massa, "Design and validation of a reconfigurable single varactor-tuned reflectarray," *IEEE Trans. Antennas Propag.*, vol. 61, no. 2, pp. 635–645, Feb. 2013.
[12] L. Cabria, J. A Garcia, A. Tazon, and J. Vassal'lo, "An active reflectarray with beamsteering capabilities," in *Proc. 18th Int. Conf. Appl. Electromagn. Commun. (ICECom'05)*, Oct. 2005, pp. 1–4.
[13] Flexwin Consortium. (2014) [Online]. Available: www.flexwin.eu
[14] V. Valenta *et al.*, From enabling technology to applications: Reconfigurable SiGe BiCMOS ICs with fully integrated RF MEMS switches for millimetre wave transceivers," in *Proc. ESA Microw. Technol. Techn. Workshop*, 2012, pp. 1–8.
[15] W. Menzel and D. Kessler, "A folded reflectarray antenna for 2d scanning," in *Proc. German Microw. Conf.*, Mar. 2009, pp. 1–4.
[16] W. Menzel and Ralf Leberer, "Folded reflectarray antennas for shaped beam applications," in *Proc. Eur. Conf. Antennas Propag.*, Nov. 2006, pp. 1–4.
[17] D. Zhou *et al.*, "New multi-layer millimetre-wave folded reflectarray antennas for satellite communications," in *Proc. Eur. Conf. Antennas Propag. (EUCAP)*, Mar. 2012, pp. 821–824.
[18] R. J. Mailloux, *Phased Array Antenna Handbook*. Norwood, MA, USA: Artech House, 2005.
[19] *Ansys HFSS V15*, 14 ed. Pittsburgh, PA, USA: Ansoft Corp., 2014.
[20] Agilent Technologies, *Agilent Network Analysis Product Note*. Santa Clara, CA, USA, 2006.
[21] D. M. Pozar, *Microwave Engineering*, 4th ed. Hoboken, NJ, USA: Wiley, 2011.
[22] R. Janaswamy and D. H. Schaubert, "Characteristic impedance of a wide slotline on low-permittivity substrates (short paper)," *IEEE Trans. Microw. Theory Techn.*, vol. 34, no. 8, pp. 900–902, Aug. 1986.
[23] P. W. Hannan, D. Lerner, and G. Knittel, "Impedance matching a phased-array antenna over wide scan angles by connecting circuits," *IEEE Trans. Antennas Propag.*, vol. 13, no. 1, pp. 28–34, Jan. 1965.
[24] R. C. Hansen, *Phased Array Antennas*. Hoboken, NJ, USA: Wiley, 2009.
[25] A. K. Bhattacharyya, *Phased Array Antennas: Floquet Analysis, Synthesis, BFNs, and Active Array Systems*. Hoboken, NJ, USA: Wiley, 2006.
[26] W. C. Chew, J. A. Kong, and L. C. Shen, "Radiation characteristics of a circular microstrip antenna," *J. Appl. Phys.*, vol. 51, no. 7, pp. 3907–3915, 1980.

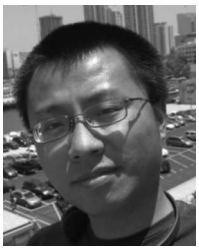

Qi Luo (S'08–M'12) was born in Chengdu, China, in 1982. He received the M.Sc. degree from the University of Sheffield, Sheffield, U.K., in 2006, and the Ph.D. degree from the University of Porto, Porto, Portugal, in 2012.

From 2012 to 2013, he worked with Surrey Space Centre, Surrey, U.K. as a Research Fellow. Currently, he is working with the School of Engineering and Digital Arts, University of Kent, Kent, U.K. as a Research Associate. His research interests include smart antennas, reflectarray, multiband microstrip antennas, and electrically small antenna design.

Steven Gao (M'01) received the Ph.D. degree from Shanghai University, Shanghai, China.

He is a Professor and Chair of RF and Microwave Engineering with the University of Kent, Kent, U.K. He has co-authored two books including *Space Antenna Handbook* (Wiley, 2012) and *Circularly Polarized Antennas* (IEEE-Wiley, 2014), authored or co-authored over 200 papers, and holds several patents in smart antennas and RF. His research interests include smart antennas, phased arrays, satellite antennas, RF/microwave/mm-wave circuits, satellite communications, UWB radars, synthetic-aperture radars, and mobile communications.

Prof. Gao is an IEEE AP-S Distinguished Lecturer and a Chair of LAPC 2013.

Chong Zhang was born in Shenyang, Liaoning, China, in 1985. He received the B.S. degree in electronics and information engineering and the M.S. degree in electromagnetic field and microwave technology from the Northwestern Polytechnical University, Xian, China, in 2008 and 2011, respectively. He is currently pursuing the Ph.D. degree in electromagnetic field and microwave technology at the same university.

His research interests include the folded reflectarray antenna and the Van Atta array.

Dawei Zhou received the Ph.D. degree in active integrated antennas from the University of Bradford, Bradford, U.K., in 2007.

He is currently working as an Antenna Specialist with Huawei Device Ltd., Beijing, China.

Dr. Zhou is a Chartered Engineer and a member of the Institution of Engineering and Technology (MIET).

Tobias Chaloun received the degree in electrical engineering with emphasis on RF and communications engineering from the University of Ulm, Ulm, Germany, from 2004 to 2010.

Since March 2010, he has been with the Institute of Microwave Techniques, University of Ulm as a Research Assistant.

Wolfgang Menzel (M'89–SM'90–F'01) received the Dipl.-Ing. degree in electrical engineering from the Technical University of Aachen, Aachen, Germany, in 1974, and the Dr.-Ing. degree in electrical engineering from the University of Duisburg, Duisburg, Germany, in 1977.

In 1989, he became a Full Professor with the Institute of Microwave Techniques, University of Ulm, Ulm, Germany. His research interests include multilayer planar circuits, antennas, millimeter-wave and microwave interconnects and packaging, and millimeter-wave sensors.

Volker Ziegler (SM'09) was born in Tuebingen, Germany, in 1971. He received the Dipl.-Ing. degree in electrical engineering and the Dr.-Ing. degree (Hons.) from the University of Ulm, Ulm, Germany, in 1997 and 2001, respectively.

Since 2007, he has been working as an EADS Expert with EADS Innovation Works, Munich, Germany, in "microwave technologies and systems" responsible for the acquisition and management of national and international research projects in the field of key microwave technologies for advanced radar and communication systems.

Mohammed Sobhy received the B.Sc. degree from the University of Cario, Cairo, Egypt, in 1956, and the Ph.D. degree from the University of Leeds, Leeds, U.K., in 1966.

He is currently an Emeritus Professor of Electronics with the University of Kent, Kent, U.K.